Electrochimica Acta 170 (2015) 33–38

Contents lists available at ScienceDirect

Electrochimica Acta

journal homepage: www.elsevier.com/locate/electacta

Application of Electrochemical Impedance for Characterising Arrays of Bi_2S_3 Nanowires

Gunta Kunakova [a,*], Juris Katkevics [a,b], Arturs Viksna [a,b], Zanda Gertnere [a], Justin Varghese [c,d], Justin D. Holmes [c,d], Donats Erts [a]

[a] Institute of Chemical Physics, University of Latvia, Raina Blvd. 19, Riga, LV-1586, Latvia
[b] Department of Analytical Chemistry, University of Latvia, Kr. Valdemara 48, LV-1013, Latvia
[c] Materials Chemistry & Analysis Group, Department of Chemistry and the Tyndall National Institute, University College Cork, Ireland
[d] Centre for Research on Adaptive Nanostructures and Nanodevices (CRANN), Trinity College Dublin, Dublin 2, Ireland

ARTICLE INFO

Article history:
Received 11 February 2015
Received in revised form 19 March 2015
Accepted 4 April 2015
Available online 18 April 2015

Keywords:
Electrochemical Impedance Spectroscopy
Nanowire
Bismuth sulphide
Anodic aluminium oxide

ABSTRACT

Electrochemical Impedance Spectroscopy (EIS) was used to characterise the electrical properties of bismuth sulphide (Bi_2S_3) nanowires (NWs) templated within anodic aluminium oxide (AAO) membranes. A specially engineered cell, with a nominal electrolyte volume of 0.1–0.2 ml, was used to hold and measure the electrochemical impedance of the fragile NW/AAO samples. An equivalent circuit model was developed to determine the filling density of nanowires within the porous templates. The EIS method can be utilised to probe the nanowire filling density in porous membranes over large sample areas, which is often unobtainable using electron microscopy and conductive atomic force microscopy techniques.

1. Introduction

Bi_2S_3 is a semiconductor with a direct band gap of 1.3 eV which has been applied as an active material in biomolecule detection [1], gas sensing [2,3] and optoelectronic devices [4]. These applications have also included the incorporation of Bi_2S_3 nanowires into ordered arrays using porous templates Anodic aluminium oxide (AAO) is one of the most frequently used templates employed to produce arrays of nanowires in combination with electrochemical, supercritical fluid and chemical vapour deposition approaches [5–8]. Several characterisation methods have been employed to determine the electrical properties and nanowire filling densities within porous membranes [5,7,9–13]. In particular, gas adsorption methods have been utilised to characterise the volume of empty nanopores within templating membranes [9] and electron microscopy techniques have been developed to characterise the structure and filling density of nanowire arrays at a local scale [5,7,8]. Conductive atomic force microscopy (C-AFM) has also been applied to determine the quality and density of the nanowires inside porous templates [10–13], although information about partly filled nanopores cannot be extracted from these data. C-AFM is also inadequate for the large scale characterisation of samples.

Electrochemical impedance spectroscopy (EIS) is widely used for characterising the properties of large area electrodes, including those coated with porous layers [14]. EIS methods have been used previously to characterise the electrical behaviour of free standing nanowires for different applications, such as electrochemical capacitors [15], photo-anodes [16] and elements for photovoltaics [17]. EIS has also been applied for resolving the electrodeposition parameters of metallic nanowires into the pores of AAO membranes and their interfacial electron transport [18–20]. However, to-date there has been no reports about the application of EIS for characterising the electrical properties and filling densities of nanowires templated within porous membranes, such as AAO, over the large areas. In this article, we detail an EIS-based method for the comprehensive and non-destructive characterisation of templated complex nanomaterials, such as arrays of assembled nanowires. Here we detail the characterisation of arrays of Bi_2S_3/AAO nanowire assemblies, through the construction of equivalent circuits and electrochemical cells, although our approach can also be applied to the analysis of the other types of templated nanomaterials.

* Corresponding author. Tel.: +371 67033875.
E-mail address: donats.erts@lu.lv (D. Erts).

http://dx.doi.org/10.1016/j.electacta.2015.04.021
0013-4686/

2. Experimental

2.1. Sample Preparation

Arrays of Bi_2S_3 nanowires were fabricated inside the pores of AAO membranes, with nominal diameters of 200 nm, by the thermolysis of the single source precursor bismuth bis(diethyldithiocarbamate) [$Bi(S_2CNEt_2)_3$]. The detailed method for synthesis of the Bi_2S_3 nanowires inside the porous AAO membranes is described in the Ref. [21]. Structural characterisation of the nanowire arrays were performed using X-ray diffraction (XRD), high resolution transmission electron microscopy (TEM), selected area electron diffraction SAED as described in detail elsewhere [21]. Initially both surfaces of the AAO membranes containing the nanowires were polished to remove reaction products from the surface. Polishing of the membranes was performed using the diamond suspensions (Buehler) with different size of the particles for each suspension. For the initial polishing, suspensions with the particle size of 6; 1; 0.5 μm were used and for the final step: 0.1 and 0.05 μm respectively. Au was then deposited on one side of the polished membranes to provide electrical contact to the nanowires within the templates. Arrays of the nanowires were visualised by scanning electron microscopy (SEM) (Hitachi S4800) at an acceleration voltage of 2 kV. The number of empty/filled pores per cm^2 was determined from the SEM images.

Conductive atomic force microscopy (C-AFM) measurements were performed using an Asylum Research MFP-3D instrument. Commercially available diamond coated DCP20 tips from NT-MDT with a nominal radius of 100 nm were used in all measurements. The C-AFM tips were grounded whilst a 10 V dc bias was applied to the sample. The topographic images of the samples were recorded in contact mode simultaneously with the current image of the same area. Energy dispersive X-ray maps were obtained using Bruker Quantax spectrometer installed on a scanning electron microscope (SEM) (Hitachi S4800) operating at accelerating voltages of 25 and 30 kV.

2.2. Electrical and Electrochemical Impedance Measurements

Samples were integrated in electrolytic cells with a total volume of between 0.1–0.2 ml (Fig. 1). For electrochemical measurements, Bi_2S_3/AAO samples were used as cathodes, Pt plates were used as anodes and Ag/AgCl was used as the reference microelectrode. A 0.1 M solution of sodium acetate (CH_3COONa) was used as the cell electrolyte. Obtaining reliable and accurate EIS data required precise adjustment (0.25–0.35 cm) of the distance between the cathode and anode. Adjustment was performed using a micrometric screw under a binocular microscope.

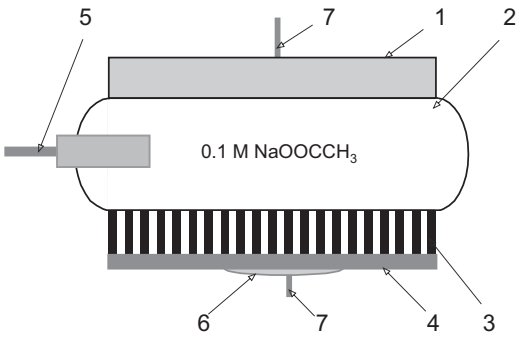

Fig. 1. Schematic representation of the electrochemical cells with a small volume (1-2 ml) of electrolyte for electrochemical impedance measurements: 1 – anode (Pt plate); 2 – electrolyte; 3 – Bi_2S_3/AAO sample; 4 – Au layer; 5–Ag/AgCl microelectrode; 6–contact; 7–Pt wire.

Before any electrochemical impedance measurements were undertaken, each sample was conditioned (immersion) in the electrolyte solution for 30 min. All measurements were performed with an "Autolab PGSTAT 30" potentiostat. The electrochemical characteristic window, kinetics and potential areas of ion mass transfer for electrochemical impedance measurement were determined from cyclic voltammograms. Impedance spectra were obtained at potentials of −0.05 V to −0.30 V and at scan frequencies ranging from 10 kHz to 0.02 Hz, using the 10 mV amplitude of sinusoidal voltage. Empty AAO membranes were measured in a similar manner. One sample was used to obtain several EIS scans; but fresh electrolyte was exchanged between the measurements of each spectrum

2.3. Analysis of Impedance Spectra

The equivalent electrical circuit was derived and impedance element values were calculated using frequency response analysis (FRA). Impedance data from the Bi_2S_3/AAO samples and empty AAO membranes were analysed using a complex plane Nyquist plot [22–24]. After successful validation of the experimental data, a Nyquist plot diagram was used to evaluate the number of elements in the Randle's equivalent circuit. Parameter fitting for the equivalent circuit elements was performed by fitting and simulation programs "RCNTRANS" and "EQUIVCRT" definition of Dr. B. A Boukamp (The FRA Windows), which are based on a non-linear least, squares methods [25].

3. Results and Discussion

Investigation of the electrochemical impedance parameters of arrays of Bi_2S_3 nanowires within the AAO membranes was conducted on samples with low (L) and high (H) pore filling densities. Filling densities, *i.e.*, the percentage of pores within the membranes containing Bi_2S_3 nanowires were determined from SEM images, over different sample areas as shown in Fig. 2. In the low density nanowire samples, 73–77% of the membrane pores were filled (Fig. 2a), compared to the high density nanowire samples, where 97–99% of the nanopores were filled (see example in Fig. 2b).

The number of filled nanopores per sample area was taken into account in the electrochemical impedance parameter calculations. Results for the samples shown in the paper are summarised in the Table 1. However, it should be noted that SEM images taken of the samples did not cover the full sample area, *i.e.* 1 cm^2. SEM analysis cannot be used to evaluate the degree of pore filling, *i.e.* pores which are only partially filled with nanowires do not run continuously through the entire length of the pores.

C-AFM images in the localised areas of the arrays of the nanowires, with a filling density of approximately 99%, highlighted the fact that not all of the nanowires seen in the topography images (Fig. 2c) were conductive (Fig. 2d) and hence did not run continuously through the full length of the nanopores. Furthermore energy dispersive X-ray mapping over the high density nanowire array samples were performed to support the presence of nanowires in the AAO templates. An example of an EDS map for a high density Bi_2S_3/AAO nanowire sample is shown in Fig. 2e, confirming that the bright spots in the SEM image refer to the positions of the Bi_2S_3 nanowires.

EIS measurements were conducted on nanowire samples and AAO membranes with the aim of obtaining information about the electrical properties of the nanowires over large areas. In order to establish the impedance measurement region, the electrochemical window was determined by measuring the cyclic voltammetric curves for arrays of Bi_2S_3/AAO nanowire samples and empty AAO

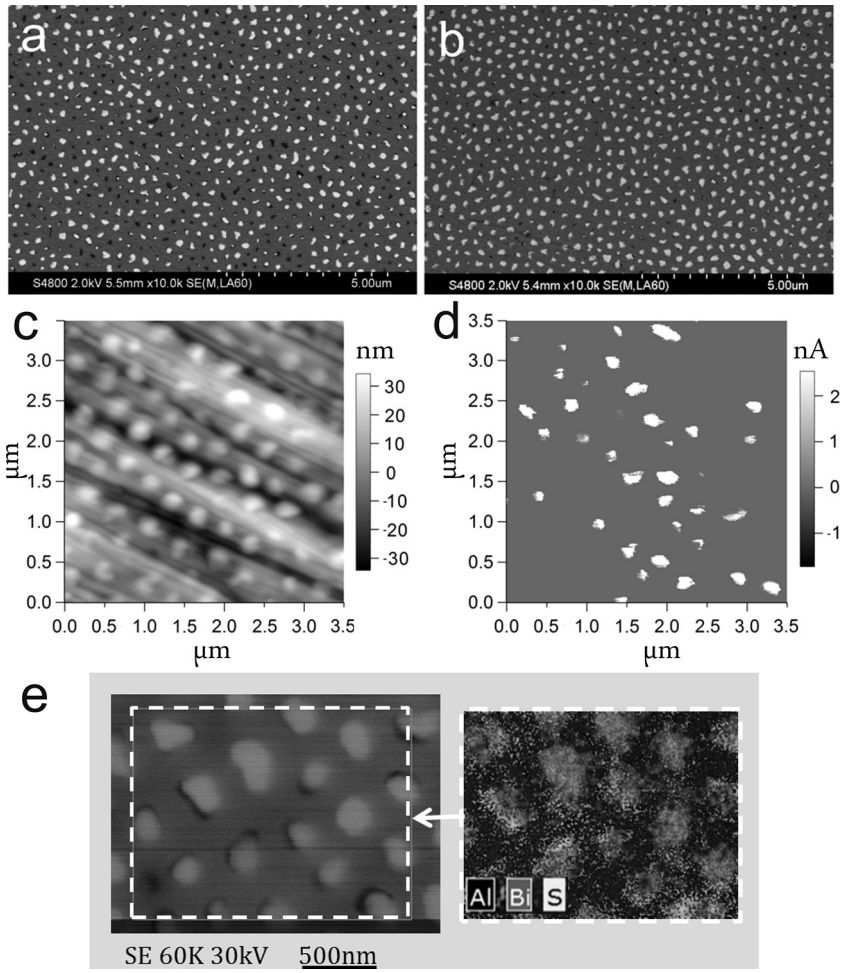

Fig. 2. Comprehensive surface analysis of the Bi_2S_3/AAO nanowire arrays: SEM images of (a) low (77 %) and (b) high (99 %) filling densities of Bi_2S_3 nanowires in AAO membranes; AFM image of high density a Bi_2S_3/AAO sample: (c) topography and (d) current mapping; (e) EDS map of high density Bi_2S_3/AAO sample (Al Kα 1.486 eV, Bi Lα 10.839 eV, S Kα 2.309 eV).

membranes (Fig. 3a). The equilibrium potential for both high and low density filled Bi_2S_3/AAO samples was found to be between −0.30 to −0.05 V. The slope of the equilibrium potential zone decreased from 6.67×10^{-7} V/dec for empty AAO membranes down to around 1.27×10^{-7} V/dec for the Bi_2S_3/AAO samples with 77% filling density, and remained practically constant for the samples with filling density of 99%.

Electrochemical impedance spectra of the Bi_2S_3/AAO nanowire samples were obtained in the equilibrium potential range of the electrochemical window. To characterise the oxidation transition equilibrium point, the cyclic voltammetric data of the Bi_2S_3/AAO nanowire arrays and AAO nanoporous samples were analysed by the Tafel slope test [14,25] (Fig. 3b, c). For a selected region NOVA software was used to calculate the Tafel slopes and the corrosion currents. The overpotential (η) was defined as the difference between the applied potential and the corrosion potential (E_{corr}).

The corrosion potential is the open circuit potential for a corroding Bi_2S_3 nanowire or AAO nanoporous wall. For large cathode overpotential ($b_c < -1$), the Tafel equation [14,25] for a cathodic reaction is given by Eq. (1):

$$\eta = \log i_{corr.} - b_c \log|i| \quad (1)$$

E_{corr} for all Bi_2S_3/AAO samples and AAO membranes was −0.12 V and −0.24 V respectively. The corrosion current density (i_{corr}) was 7.3×10^{-7} A cm^{-2} and 9.2×10^{-7} A cm^{-2} for all Bi_2S_3/AAO and AAO membranes respectively. The calculated values of coefficient b_c were 0.084 V and 0.181 V for the Bi_2S_3/AAO nanowire arrays and empty AAO membranes respectively.

Nyquist diagrams for empty and Bi_2S_3 filled AAO samples are shown in the Fig. 4 (curves 1–3). For the empty AAO membrane, the impedance spectra were similar and comparable at voltage-s between −0.10 to −0.20 V, for all of the frequency intervals

Table 1
Characteristics of AAO and AAO/Bi_2S_3 nanowire samples.

Parameters	AAO	Low density	High density
Sample area, mm^2	7.04	7.68	1.45
Quantity of nanopores or nanowires/ cm^2	7.50E + 08	6.90E + 08	6.40E + 08
Filled nanopores, %	0	77	99

Table 2
Fitting parameters used to simulate the EIS data for AAO nanoporus sample in 0.1 M acetate solution at −0.20 V potential after 30 min immersion, equivalent circuit $R_e(R_2Q_1)$.

Elements, Unit	Parameter	$E_{st.}$ Error, %
R_e / (W cm^2)	97	0.5
R_2 / (kW cm^2)	41	0.8
Q_1 / (mF cm^{-2})	8.14	0.9
n_1	0.821	0.2

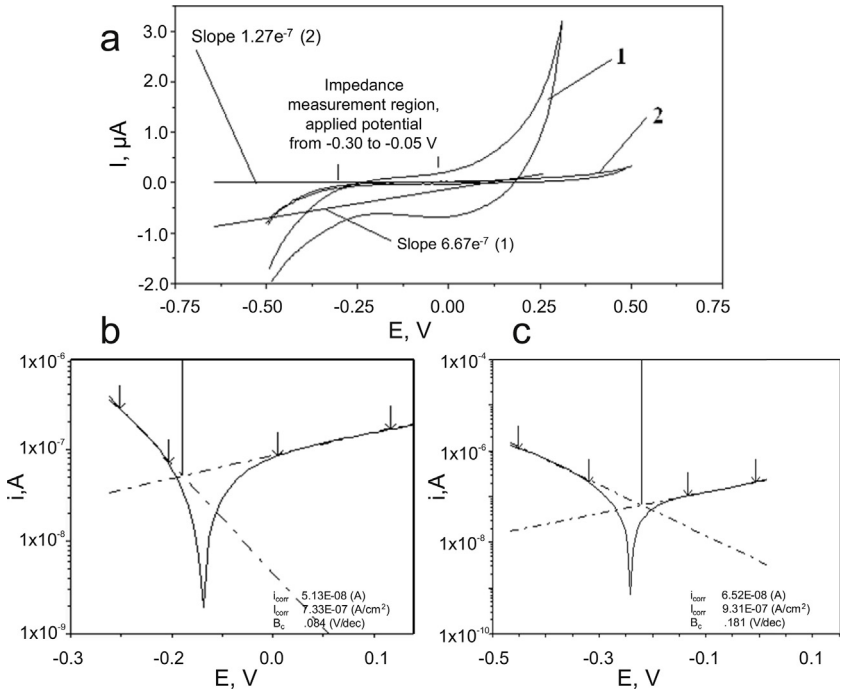

Fig. 3. (a) Cyclic voltammetric curves after 30 min immersion in the electrolyte: 1–AAO membrane; 2–low density Bi_2S_3/AAO nanowire array (77% pore filling); Tafel slope analysis for (b) high density Bi_2S_3/AAO array and (c) empty AAO membrane after 30 min of immersion in 0.1 M CH_3COONa.

between 10 kHz to 0.02 Hz. However, for the Bi_2S_3/AAO samples the impedance spectra were similar and comparable at high frequencies (10.0 to 1.5 kHz), but different at low frequencies (0.1 Hz to 0.02 Hz). Differences in the impedance spectra were more pronounced at high filling densities (Fig. 5, curve 3) and high voltages. The difference in the impedance spectra at low frequencies and at different voltages has previously been observed for Bi_2S_3 nanoparticles [26]. Since impedance spectra at low frequencies for the AAO membranes filled with Bi_2S_3 nanowires exhibited similar behavior to Bi_2S_3 nanoparticles, this indicates that variances in the EIS spectra at low frequencies for filled AAO membranes is due to the presence of Bi_2S_3 inside the nanopores.

At the beginning EIS data for all samples were analysed by widely used mathematical equivalent circuit diversiform (models, formula) for porous electrodes, *i.e.* circuit description 1–R(RQ), 2–R(RQ)(RQ) and 3–R([R(RQ)]Q) [14,25], composed from a combination of resistances (R) and capacitances (Q). For the empty AAO membranes, only one kink was present in the Bode plots (Fig. 5, curve 4), indicating the presence of a single RQ component. Hence only an R(RQ) circuit was applied in further analysis.

Errors of calculated element values (Table 2) of equivalent circuit R(RQ) (Fig. 6a) for the empty AAO membranes were below 1%, indicating that for the empty AAO membranes simple R(RQ) circuit can be applied to the EIS spectra analysis.

The presence of two kinks in the Bode plots (Fig. 5, curves 5, 6) for Bi_2S_3 nanowire arrays with both high and low filling densities confirmed the existence of two parallel RQ structures and therefore both R(RQ)(RQ) and R([R(RQ)]Q) [14,25] circuits were considered for EIS spectra analysis.

Table 3 summarizes fitting parameters of the equivalent circuit R(RQ)(RQ). Estimated errors for some of the parameters were 100 % for both high and low density nanowire arrays, confirming that this equivalent circuit could not be used for EIS data analysis. Although errors of R([R(RQ)]Q) circuit elements were lower in comparison to an R(RQ)(RQ) circuit, an error of 38 % for the electrolyte resistance (R_e) was too large for EIS data analysis of the Bi_2S_3nanowire arrays.

We have optimised the equivalent circuit of porous electrodes [14] for our system by ordering elements of the circuit $R_e(C_{\ell 1}[R_{\ell 1}(Z_f C_{d\ell})])$ to $R_e([R_2(R_3Q_2)]Q_1)$ (Fig. 6, b, c), where R_e is the electrolyte resistance; R_2 is the resistance in the AAO

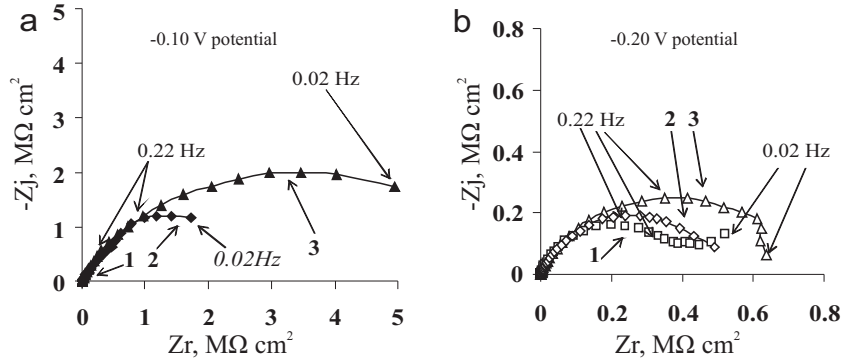

Fig. 4. Nyquist diagram for Bi_2S_3/AAO nanowire arrays and AAO nanopore sample after 30 min immersion in 0.1 M CH_3COONa at frequency interval 10 kHz – 0.02 Hz and different applied potentials: a –-0.10 V; b –-0.20 V; 1–AAO sample; 2–low density Bi_2S_3/AAO nanowire sample; 3–high density Bi_2S_3/AAO nanowire sample.

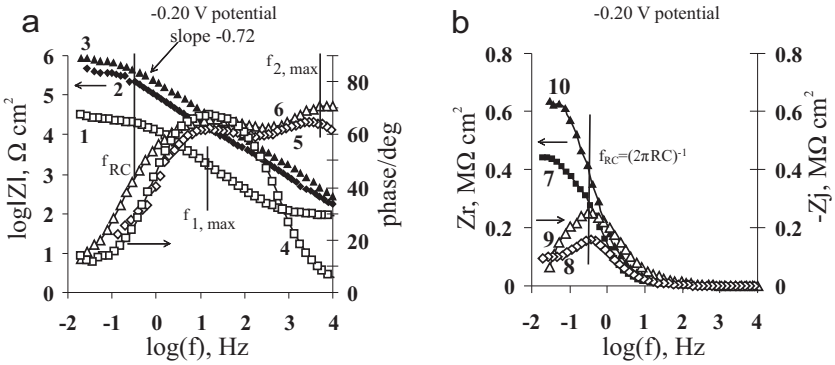

Fig. 5. Bode diagram for the empty AAO and Bi_2S_3/AAO nanowire array samples after 30 min immersion in aqueous acetate (0.10 mol · L^{-1}), applied potential scan -0.20 V: 1, 4, 7, 8–AAO sample; 2, 5–low density Bi_2S_3/AAO nanowire sample; 3, 6, 9, 10–high density Bi_2S_3/AAO nanowire samples; 1, 2, 3–modulus impedance; 4, 5, 6–phase angle; 7, 10–real impedance part; 8, 9–imaginary impedance part.

nanopores, which is the combination of the resistance from the electrolyte in the nanopores and the resistance of the nanowires; R_3 and Q_2 is the resistance and capacitance of the double layer between the electrolyte/Bi_2S_3 nanowire samples and the Au electrode respectively; C_1 is the capacitance of the AAO pore walls. As can be seen from the fitted data presented in Table 4, errors of all circuit $R_e([R_2(R_3Q_2)]C_1)$ elements were below 8%, hence this model can be applied for the analysis of arrays of Bi_2S_3 nanowires with different filling densities. The value of R_3, which characterises the resistance of the double layer between the nanowires in the nanopores and the Au electrode increases from 0.54 MΩ cm^2 for a low density Bi_2S_3/AAO sample, up to 1.03 MΩ cm^2 for a high density sample. This increase in the double layer resistance is probably caused by the formation of a Schottky barrier between the Bi_2S_3 and Au surfaces. The value of R_2, which characterises the total resistance of a Bi_2S_3/AAO nanowire sample, increases as a function of nanowire filling density, *i.e.* from 1.12 kΩ cm^2 up to 2.01 kΩ cm^2, for low and high density samples, respectively. According to B. A. Boukamp classification of capacitance [27], the capacitance values between 1–10 nF · cm^{-2} signifies the presence of grain boundaries within the nanowires, whilst values between 0.1–10 μF · cm^{-2} are characteristic of a double layer/space charges. Hence, a capacitance (C_1) value of 10 nF · cm^{-2} for the low and 60 nF · cm^{-2} for the high density arrays of the nanowires indicates that the ends of the Bi_2S_3 nanowires act as grain boundaries. A calculated value for the element Q_2, which is characteristic of the capacitance of the double layer between the Bi_2S_3 nanowires and the Au electrode (Table 4), was 41.2 μF · cm^{-2} for low density nanowire arrays, decreasing by several orders of magnitude for high density nanowire arrays, *e.g.* 0.97 μF cm^{-2} for 99% filled membranes.

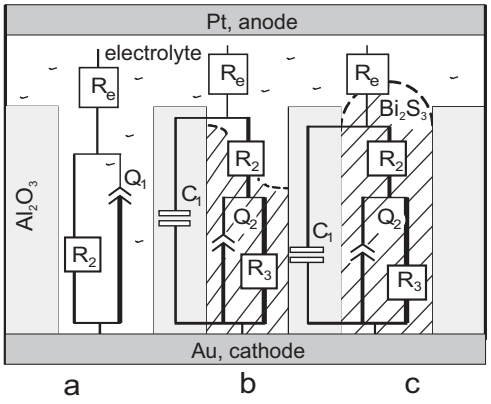

Fig. 6. Equivalent circuits for electrochemical impedance elements calculation: (a) model for the empty AAO membrane, R(RQ), (b, c) model for the Bi_2S_3/AAO nanowire array samples, $R_e([R_2(R_3Q_2)]C_1)$.

Table 3
Fitting parameters used to simulate the EIS data for the Bi_2S_3/AAO array sample in 0.1 M acetate solution at potential −0.20 V after 30 min immersion, equivalent circuit $R_e(R_2Q_1)(R_3Q_2)$.

Element, Units	Low density	Error, %	High density	Error, %
R_e / (Ω cm^2)	40	100	55	23
R_2 / kΩ cm^2)	10.9	100	864	20.7
Q_1 / (mF cm^{-2})	3	100	15.4	37.4
n_1	0.71	50.4	0.695	4.1
R_3/ MΩ cm^2)	0.907	20.7	0.146	100
Q_2 (mF cm^{-2})	26.2	3.1	61.4	65.5
n_2	0.72		0.945	19.2

Bode plots diagrams (Fig. 5) were also analysed to characterise the electrochemical parameters of the materials. These diagrams for empty AAO membranes and Bi_2S_3/AAO nanowire arrays showed that EIS spectra could be measured at an applied potential of −0.20 V and below. EIS spectra could also be measured at −0.1 V for empty AAO samples. The changes in the impedance phase angle as a function of frequency for empty AAO membranes was fitted with one time constant, whereas for the low and high density arrays of nanowires could be fitted with two time constants ($f_{1,max}$ and $f_{2,max}$) (Fig. 5a). The slope values f_{RC} and $R+R_e$ were calculated for the empty AAO membrane and all of the arrays of Bi_2S_3/AAO nanowires. The slope of the impedance modulus Z frequency at the transition point, on a log – log scale (Fig. 5a), was between −0.72–−0.74 for empty AAO membranes and for the low and high density Bi_2S_3 nanowire samples. The time constant for the empty AAO nanowire arrays $f_{RC} = (2pRC)^{-1} = 0.38–0.42\ s^{-1}$ was identical with one of the time constants for the low and high density Bi_2S_3/AAO samples (Fig. 5a). Despite the different structure of the materials, for the arrays of Bi_2S_3 nanowires large volumes of empty space

Table 4
Fitting parameters used to simulate the EIS data for the Bi_2S_3/AAO array sample in 0.1 M acetate solution at −0.20 V potential after 30 min immersion, equivalent circuit $R_e([R_2(R_3Q_2)]C_1$.

Element, Units	Low density	$E_{st.}$Error, %	High density	$E_{st.}$Error, %
R_e / (W cm^2)	87	6	68	7.9
R_2 / (kW cm^2)	1.12	1.8	2.01	4.9
R_3 / (MW cm^2)	0.54	5.1	1.03	5.1
Q_2 / (mF cm^{-2})	41.2	3.8	0.97	1.2
n_2	0.681	1.4	0.712	0.4
C_1 / (nF cm^{-2})	10	4.4	60	1.5

were filled with the electrolyte. The second time constant (Fig. 5b) determined for the Bi_2S_3 nanowire arrays $f_{RC} = 0.29$ s^{-1} was characteristic of the Bi_2S_3 material.

Maximal impedance modulus ($R_e + R$) at low frequencies were related to the reactive circuit with values of 0.04 $M\Omega\,cm^2$, 0.37–0.42 $M\Omega\,cm^2$ and 0.50–0.87 $M\Omega\,cm^2$ for the empty AAO, low and high density nanowire arrays respectively (Fig. 5a). The rising impedance modulus with increasing nanowire filling density can be explained by changes in the sample structure containing a mixture of four components: electrolyte, Bi_2S_3 nanowires, AAO pore walls and the nanopores themselves. The relationship between these components changes the impedance. The increase of the impedance modulus by increasing nanowire filling density can be used to quantify the filling density over large areas of nanowire arrays grown in nanoporous templates.

4. Conclusions

Experimental data has shown that the EIS parameters of a cell containing an AAO membrane or an array of AAO/Bi_2S_3 nanowires can be interpreted in terms of the equivalent circuit denoted as $R_e([R_2(R_3Q_2)]C_1)$, where R_e is the electrolyte resistance; R_2 is the resistance in the AAO nanopores (obtained from the resistance of the electrolyte in nanopores and resistance of the nanowires); R_3 and Q_2 are the resistance and capacitance of the double layer between the electrolyte/Bi_2S_3 nanowire samples and the Au electrode respectively; C_1 is the capacitance of the AAO pore walls. The values of equivalent circuit and the impedance modulus have been successfully used to characterise the filling density of arrays of Bi_2S_3 nanowire within an AAO membrane. Electrochemical impedance spectroscopy could be considered as an alternative method for determining the filling density and resistance of templated nanowires arrays, over large areas, which is difficult to achieve using other techniques. The approach could also be utilised for characterising arrays of other nanomaterials, *e.g.* nanotubes, within other templates, *e.g.* polymer membranes. In order to characterize other templated nanomaterials with presented approach, one has to consider several aspects such as compatibility of materials with the electrolyte and formation of the electrical contact with the nanomaterial sample. Depending on material properties, an increase of frequency interval may be required.

To summarize, simple method for evaluation of the pore filling density of the nanoporous samples is based on determination and comparing of impedance modulus of unknown sample with impedance moduli of 2 standards – empty and fully filled nanoporous sample. In absence of standards, difference in filling levels can be determined by comparison of impedance moduli of different samples.

Acknowledgements

This work has been supported by ERAF project No. 2010/0251/2DP/2.1.1.1.0/10/APIA/VIAA/096. GK acknowledges the European Social Fund within the project «Support for Doctoral Studies at University of Latvia». JDH and JV acknowledge financial support from Science Foundation Ireland (SFI) (Grant: 09/IN1/I2602).

References

[1] L. Cademartiri, F. Scotognella, P.G. O'Brien, B.V. Lotsch, J. Thomson, S. Petrov, N. P. Kherani, G.A. Ozin, Cross-linking Bi_2S_3 ultrathin nanowires: a platform for nanostructure formation and biomolecule detection, Nano Lett. 9 (2009) 1482.
[2] H. Li, J. Yang, J. Zhang, M. Zhou, Facile synthesis of hierarchical Bi_2S_3 nanostructures for photodetector and gas sensor, RSC Adv. 2 (2012) 6258.
[3] A.D. Schricker, M.B. Sigman, B.A. Korgel, Electrical transport,Meyer–Neldel rule and oxygen sensitivity of Bi_2S_3 nanowires, Nanotechnology 16 (2005) S508.
[4] H. Bao, C.M. Li, X. Cui, Q. Song, H. Yang, J. Guo, Single-crystalline Bi_2S_3 nanowire network film and its optical switches, Nanotechnology 19 (2008) 335302.
[5] M.J. Zheng, L.D. Zhang, G.H. Li, W.Z. Shen, Fabrication and optical properties of large-scale uniform zinc oxide nanowire arrays by one-step electrochemical deposition technique, Chem. Phys. Lett. 363 (2002) 123.
[6] T.A. Crowley, K.J. Ziegler, D.M. Lyons, D. Erts, H. Olin, M.A. Morris, J.D. Holmes, Synthesis of metal and metal oxide nanowire and nanotube arrays within a mesoporous silica template, Chem. Mater. 15 (2003) 3518.
[7] T. Shimizu, T. Xie, J. Nishikawa, S. Shingubara, S. Senz, U. Gösele, Synthesis of vertical high-density epitaxial Si(100) nanowire arrays on a Si(100) substrate using an anodic aluminum oxide template, Adv. Mater. 19 (2007) 917.
[8] L. Liu, W. Lee, Z. Huang, R. Scholz, U. Gösele, Fabrication and characterization of a flow-through nanoporous gold nanowire/AAO composite membrane, Nanotechnology 19 (2008) 335604.
[9] L.P. Barrett, L.G. Joyner, P.P. Halenda, The determination of pore volume and area distributions in porous substances, J. Am. Chem. Soc. 73 (1951) 373.
[10] P. Birjukovs, N. Petkov, J. Xu, J. Švirksts, J.J. Boland, J.D. Holmes, D. Erts, Electrical characterization of bismuth sulfide nanowire arrays by conductive atomic force microscopy, J. Phys. Chem. C 112 (2008) 19680.
[11] D. Erts, B. Polyakov, B. Daly, M.A. Morris, S. Ellingboe, J. Boland, J.D. Holmes, High density germanium nanowire assemblies: contact challenges and electrical characterization, J. Phys. Chem. B 110 (2006) 820.
[12] K. Wang, P. Birjukovs, D. Erts, R. Phelan, M.A. Morris, H. Zhou, J.D. Holmes, Synthesis and characterisation of ordered arrays of mesoporous carbon nanofibre, J. Mater. Chem. 19 (2009) 1331.
[13] N. Petkov, P. Birjukovs, R. Phelan, M.A. Morris, D. Erts, J.D. Holmes, Growth of ordered arrangements of one-dimensional germanium nanostructures with controllable crystallinities, Chem. Mater. 20 (2008) 1902.
[14] M.E. Orazem, B. Tribollet, ECS-The Electrochemical Society 159 (2008) 533.
[15] F. Zhang, C. Yuan, X. Lu, L. Zhang, Q. Che, X. Zhang, Facile growth of mesoporous Co_3O_4 nanowire arrays on Ni foam for high performance electrochemical capacitors, J. of Power Sources 203 (201) (2012) 250.
[16] X. Gan, X. Li, X. Gao, F. Zhuge, W. Yu, ZnO nanowire/TiO_2 nanoparticle photoanodes prepared by the ultrasonic irradiation assisted dip-coating method, Thin Solid Films 518 (2010) 4809.
[17] C.W. Kung, H.W. Chen, C.Y. Lin, K.C. Huang, R. Vittal, K.C. Ho, CoS acicular nanorod arrays for the counter electrode of an efficient dye-sensitized solar cell, ACS Nano 6 (2012) 7016.
[18] G. Sharma, M.V. Pishko, C.A. Grimes, Fabrication of metallic nanowire arrays by electrodeposition into nanoporous alumina membranes: effect of barrier layer, J. Mater. Sci. 42 (2007) 4738.
[19] X.Y. Zhang, D. Li, L. Bourgeois, H.T. Wang, P.A. Webley, Direct electrodeposition of porous gold nanowire arrays for biosensing applications, Chem. Phys. Chem. 10 (2009) 436.
[20] C.H. Liang, K. Terabe, T. Hasegawa, M. Aono, N. Iyi, Anomalous phase transition and ionic conductivity of AgI nanowire grown using porous alumina template, J. Appl. Phys. 102 (2007) 124308.
[21] J. Xu, N. Petkov, X. Wu, D. Iacopino, A.J. Quinn, G. Redmond, T. Bein, M.A. Morris, J.D. Holmes, Oriented growth of single-crystalline Bi_2S_3 nanowire arrays, Chem. Phys. Chem. 8 (2007) 235.
[22] R. Sabino, D.S. Azambuja, R.S. Gonçalves, Electrochemical behavior of aluminum alloy AA2024 in aqueous solutions in the presence of caffeine, J. Solid State Electrochem. 14 (2010) 1255.
[23] I.U.P.A.C. Recommendations, Impedances of electrochemical systems: terminology, nomenclature and representation, Pure Appl Chem. 66 (1994) 1831.
[24] A. Lasia, Electrochemical Impedance Spectroscopy and its Applications, in: B.E. Conway, J. Bockris, R.E. White (Eds.), Modern Aspects of Electrochemistry, 32, Kluwer Academic/Plenum Publishers, New York, 1999, pp. 143.
[25] Release notes for General purose electrochemical system (GPES) for Windows –version 4.9.007 and Frequency response analysis (FRA) for Windows –version 4.9.007. 2007 Eco Chemie: www.ecochemie.nl.
[26] K.A.Z. Abuthahir, R. Jagannathan, Reverse-loop impedance profile in Bi_2S_3 quantum dots, Mater. Chem. Phys. 121 (2010) 184.
[27] B.A. Boukamp, Electrochemical Impedance Spectroscopy, Nano-Electrocatalysis, U. Leiden, 24-28 Nov. (2008) EIS, 61. p.